Transmission and time delay properties of an integrated system consisting of atomic vapor cladding on top of a micro ring resonator

Liron Stern[1] and Uriel Levy[1,*]

[1]*Department of Applied Physics, The Benin School of Engineering and Computer Science, The Center for Nanoscience and Nanotechnology, The Hebrew University of Jerusalem, Jerusalem, 91904, Israel*
[*]*ulevy@cc.huji.ac.il*

Abstract: In this paper we analyze the transmission and time delay properties of light propagating through a microring resonator (MRR) consisting of a solid core waveguide surrounded by an atomic vapor cladding. Using the atomic effective susceptibility of Rubidium we derive the complex transmission spectrum of the integrated system. We show, that when the system is under-coupled, the transmission can exceed the standalone MRR's background transmission and is accompanied by enhanced positive time delay. It is shown that in this case the contrast of the atomic lines is greatly enhanced. This allows achieving high optical densities at short propagation length. Furthermore, owing to its features such as small footprint, high tunability, and high delay-transmission product, this system may become an attractive choice for chip scale manipulations of light.

©2012 Optical Society of America

OCIS codes: (020.1335) Atom optics; (130.3120) Integrated optics devices; (230.5750) Resonators.

References and links

1. J. Vanier and C. Mandache, "The passive optically pumped Rb frequency standard: the laser approach," Appl. Phys. B **87**(4), 565–593 (2007).
2. I. K. Kominis, T. W. Kornack, J. C. Allred, and M. V. Romalis, "A subfemtotesla multichannel atomic magnetometer," Nature **422**(6932), 596–599 (2003).
3. M. M. Kash, V. A. Sautenkov, A. S. Zibrov, L. Hollberg, G. R. Welch, M. D. Lukin, Y. Rostovtsev, E. S. Fry, and M. O. Scully, "Ultraslow Group Velocity and Enhanced Nonlinear Optical Effects in a Coherently Driven Hot Atomic Gas," Phys. Rev. Lett. **82**(26), 5229–5232 (1999).
4. A. M. Marino, R. C. Pooser, V. Boyer, and P. D. Lett, "Tunable delay of Einstein-Podolsky-Rosen entanglement," Nature **457**(7231), 859–862 (2009).
5. S. Knappe, L. Liew, V. Shah, P. Schwindt, J. Moreland, L. Hollberg, and J. Kitching, "A microfabricated atomic clock," Appl. Phys. Lett. **85**(9), 1460 (2004).
6. F. Benabid, F. Couny, J. C. Knight, T. A. Birks, and P. S. J. Russell, "Compact, stable and efficient all-fibre gas cells using hollow-core photonic crystal fibres," Nature **434**(7032), 488–491 (2005).
7. W. Yang, D. B. Conkey, B. Wu, D. Yin, A. R. Hawkins, and H. Schmidt, "Atomic spectroscopy on a chip," Nat. Photonics **1**(6), 331–335 (2007).
8. T. Baluktsian, C. Urban, T. Bublat, H. Giessen, R. Löw, and T. Pfau, "Fabrication method for microscopic vapor cells for alkali atoms," Opt. Lett. **35**(12), 1950–1952 (2010).
9. A. Sargsyan, C. Leroy, Y. Pashayan-Leroy, R. Mirzoyan, A. Papoyan, and D. Sarkisyan, "High contrast D1 line electromagnetically induced transparency in nanometric-thin rubidium vapor cell," Appl. Phys. B **105**(4), 767–774 (2011).
10. L. Stern, B. Desiatov, I. Goykhman, and U. Levy, "Evanescent light-matter Interactions in Atomic Cladding Wave Guides," arXiv:1204.0393 (2012).
11. S. M. Spillane, G. S. Pati, K. Salit, M. Hall, P. Kumar, R. G. Beausoleil, and M. S. Shahriar, "Observation of Nonlinear Optical Interactions of Ultralow Levels of Light in a Tapered Optical Nanofiber Embedded in a Hot Rubidium Vapor," Phys. Rev. Lett. **100**(23), 233602 (2008).
12. S. M. Hendrickson, M. M. Lai, T. B. Pittman, and J. D. Franson, "Observation of Two-photon Absorption at Low Power Levels Using Tapered Optical Fibers in Rubidium Vapor," Phys. Rev. Lett. **105**(17), 173602 (2010).

#176246 - $15.00 USD Received 14 Sep 2012; revised 15 Nov 2012; accepted 16 Nov 2012; published 4 Dec 2012

13. K. Saha, V. Venkataraman, P. Londero, and A. L. Gaeta, "Enhanced two-photon absorption in a hollow-core photonic-band-gap fiber," Phys. Rev. A **83**(3), 033833 (2011).
14. K. Zhao and Z. Wu, "Regionally specific hyperfine polarization of Rb atoms in the vicinity (¬10^{−5}cm) of surfaces," Phys. Rev. A **71**(1), 012902 (2005).
15. H. Wang, D. J. Goorskey, W. H. Burkett, and M. Xiao, "Cavity-linewidth narrowing by means of electromagnetically induced transparency," Opt. Lett. **25**(23), 1732–1734 (2000).
16. J. Zhang, G. Hernandez, and Y. Zhu, "Slow light with cavity electromagnetically induced transparency," Opt. Lett. **33**(1), 46–48 (2008).
17. J. Guo, J. Cooper, A. Gallagher, and M. Lewenstein, "Theory of selective reflection spectroscopy," Opt. Commun. **110**(1-2), 197–208 (1994).
18. G. Nienhuis, F. Schuller, and M. Ducloy, "Nonlinear selective reflection from an atomic vapor at arbitrary incidence angle," Phys. Rev. A **38**(10), 5197–5205 (1988).
19. R. Kondo, S. Tojo, T. Fujimoto, and M. Hasuo, "Shift and broadening in attenuated total reflection spectra of the hyperfine-structure-resolved D_{2} line of dense rubidium vapor," Phys. Rev. A **73**(6), 062504 (2006).
20. J. Guo, J. Cooper, and A. Gallagher, "Selective reflection from a dense atomic vapor," Phys. Rev. A **53**(2), 1130–1138 (1996).
21. D. A. Steck, "Rubidium 87 D Line Data," *http://steck.us/alkalidata*, (unpublished)
22. L. Weller, R. J. Bettles, P. Siddons, C. S. Adams, and I. G. Hughes, "Absolute absorption on the rubidium D1 line including resonant dipole–dipole interactions," J. Phys. At. Mol. Opt. Phys. **44**(19), 195006 (2011).
23. P. Siddons, C. S. Adams, C. Ge, and I. G. Hughes, "Absolute absorption on rubidium D lines: comparison between theory and experiment," J. Phys. At. Mol. Opt. Phys. **41**(15), 155004 (2008).
24. U. Levy, K. Campbell, A. Groisman, S. Mookherjea, and Y. Fainman, "On-chip microfluidic tuning of an optical microring resonator," Appl. Phys. Lett. **88**(11), 111107 (2006).
25. J. Heebner, A. Vincent Wong, A. Schweinsberg, R. W. Boyd, and D. J. Jackson, "Optical transmission characteristics of fiber ring resonators," IEEE J. Quantum Electron. **40**(6), 726–730 (2004).
26. R. M. Camacho, M. V. Pack, and J. C. Howell, "Low-distortion slow light using two absorption resonances," Phys. Rev. A **73**(6), 063812 (2006).
27. L. Wang, "Causal "all-pass" filters and Kramers–Kronig relations," Opt. Commun. **213**(1-3), 27–32 (2002).
28. G. Müller, M. Müller, A. Wicht, R.-H. Rinkleff, and K. Danzmann, "Optical resonator with steep internal dispersion," Phys. Rev. A **56**(3), 2385–2389 (1997).
29. M. Soljačić, E. Lidorikis, L. V. Hau, and J. D. Joannopoulos, "Enhancement of microcavity lifetimes using highly dispersive materials," Phys. Rev. E Stat. Nonlin. Soft Matter Phys. **71**(2), 026602 (2005).
30. D. Goldring, U. Levy, and D. Mendlovic, "Highly dispersive micro-ring resonator based on one dimensional photonic crystal waveguide design and analysis," Opt. Express **15**(6), 3156–3168 (2007).
31. D. Goldring, U. Levy, I. E. Dotan, A. Tsukernik, M. Oksman, I. Rubin, Y. David, and D. Mendlovic, "Experimental measurement of quality factor enhancement using slow light modes in one dimensional photonic crystal," Opt. Express **16**(8), 5585–5595 (2008).
32. D. K. Sparacin, C. Y. Hong, L. C. Kimerling, J. Michel, J. P. Lock, and K. K. Gleason, "Trimming of microring resonators by photooxidation of a plasma-polymerized organosilane cladding material," Opt. Lett. **30**(17), 2251–2253 (2005).

1. Introduction

Atomic vapor cells consisting of rubidium (Rb) or Cesium are extensively used both in industry and research for myriad of applications such as atomic clocks [1], magnetometers [2], slow light [3], and quantum computation [4]. In the recent years a vast effort in miniaturizing atomic vapor cells is taking place [5–13]. Such Integrated photonic-vapor devices may provide efficient light-vapor applications due to the reduction in size and power consumption of the traditional vapor cells. Additionally, such systems show for benchmarking fundamental surface [14] and linear and non-linear [10–13] light-matter interactions, in dimensions that were previously unattainable.

When considering miniaturized light-vapor interactions on a chip scale, one approach would to be to integrate a vapor cell above a photonic circuit, where the interaction would take place via the evanescent decaying tail of the propagating mode supported by the photonic waveguide. Using this approach, one can consider a myriad of light guiding structures that can provide different types of interaction. In addition, this approach provides the ability to miniaturize the whole light-matter interaction apparatus, i.e. the platform enables integration and miniaturization of the atomic cell as well as the light's preparation, manipulation and detection. Amongst such structures, the integration of a vapor cell above a micro ring

#176246 - $15.00 USD Received 14 Sep 2012; revised 15 Nov 2012; accepted 16 Nov 2012; published 4 Dec 2012
(C) 2012 OSA

resonator (MRR) is much desired due to the benefits in enhancement light mater interactions as well as the interesting coupling of the dispersion of the MRR and vapor.

In this paper, we theoretically investigate such combined system, consisting of Rubidium (Rb) vapor integrated above a silicon nitride MRR which is coupled to a bus waveguide. An illustration of such a combined device is presented in Fig. 1(a), where a MRR with a bonded Rubidium cell is shown. Although the basic intracavity properties of vapor-cavity systems were previously investigated, such as the effect of intracvity dispersion [15], and enhancement of slow light in a cavity [16], this paper provides the fist study of a combined system consisting of vapor interacting with the evanescent field of a guided mode resonator. Specifically, we investigate the transmission and time delay properties of a Rb serving as the atomic cladding of an MRR. We use the effective atomic cladding susceptibility taking into account different broadening mechanisms as well as the dephasing (quenching) of the atoms on the wave guide's surface in order to calculate the complex effective index of the combined system guided mode. With these results, we analyze the transmission and time delay properties of the combined system as a function of the coupling conditions between the bus waveguide and the MRR. We show that the transmission of the proposed system exhibits resonant lines with enhanced contrast. As a result, high effective optical densities become achievable on a chip scale device. Moreover, we show both qualitatively and quantitatively, that when the intrinsic loss rate of the MRR exceeds the coupling rate to the MRR (the under-coupled regime) one can achieve enhanced time delay (slow light) accompanied with enhanced transmission, whereas in the opposite case where the coupling rate to the MRR exceeds the intrinsic loss rate (over-coupled regime) this scenario is inverted, i.e. a negative time delay (fast light) accompanied with decreased transmission is obtained.

2. Atomic cladding index of refraction and atomic cladding wave-guide effective index

In Fig. 1(b) we illustrate the cross section of a nitride wave guide, with a bottom cladding of silica, and top and side cladding of Rb vapor. We coin this structure as an atomic cladding wave guide (ACWG). The waveguide dimensions were chosen as a compromise between the requirement for dense integration from one hand and the desire for strong light-matter interactions, i.e. the need for significant interaction of light with the surrounding atoms, requiring a substantial portion of the optical mode to reside in the cladding. A Rb vapor is illustrated as ballistically striking the waveguide, and reflecting form its surface. Due to this thermal motion of the atoms with respect to the surface, a naive model that uses the bulk complex dispersion of Rb as a cladding layer, and calculate the perturbation resulted by the presence of the Rb vapor given the fraction of the mode residing in this cladding area isn't sufficient. Instead, one should obtain an effective cladding complex index of refraction that takes into consideration the atomic wall collisions, the finite time of interaction due to the evanescent tail, and the enhanced Doppler broadening. In fact, a similar effective index of refraction has been considered in the case of reflection from a dielectric-vapor boundary [14,17–20]. Specifically, the case of attenuated total internal reflection (ATIR) [14,18,19] can be exploited to obtain a guided effective index of refraction. Recently we have demonstrated the feasibility of such a device, and have found the formalism of such an effective susceptibility to be with good agreement with our fabricated device [10].

In order to find the refractive index of such an atomic cladding we solve the optical Bloch equations, with a boundary condition of total dephasing (quenching) when an atom strikes the waveguide wall, with no correlation between incoming and outgoing atoms. The first order solution is separated into a steady state solution, for the atoms moving toward the wall and a transient solution for the atoms moving from the wall. Using these two solutions, It can be shown that the first order susceptibility is given by the following expression [14,18,19]:

$$\chi(\nu)=\frac{e^2}{\pi\varepsilon_0 m_e}\sum_{i=1,2}C_i\sum_{F,F'}\frac{Nf_{FF'}}{2(2I+1)\nu_{F_i',F_i}}\int_{-\infty}^{\infty}dv_z\int_0^{\infty}dv_t\,\frac{W(v_z,v_t)}{-2\pi\Delta\nu-k_z v_z-i(\gamma-ik_t v_t)} \qquad (1)$$

#176246 - $15.00 USD Received 14 Sep 2012; revised 15 Nov 2012; accepted 16 Nov 2012; published 4 Dec 2012
(C) 2012 OSA

Where, N is the density of atoms, e the electric charge of an electron, ε_0 the vacuum permittivity, m_e is the electron mass, C_i is the occupation ratio (In this paper we assume Rb in natural abundance, i.e. 72.17% of ^{85}Rb and 27.83% of ^{87}Rb.), $\nu_{Fi'Fi'}$ is the transition frequency from a level with total angular momentum F to an excited state with momentum F', v_z and v_t are the atomic velocities in the propagation direction *z,* and the transverse direction respectively, *W* is the normalized velocity distribution, k_z and k_t represent the momentum of the evanescent field along the propagation direction and the transverse direction respectively. 2γ is the natural full-width half maximum line-width and $\Delta\nu$ the frequency detuning from the transition frequency. The oscillator strength $f_{FF'}$ are defined as follows:

$$f_{FF'} = fW^2(J'F'JF;I1)(2F'+1)(2F+1)/(2I+1) \qquad (2)$$

Where *f* is the D1 or D2 oscillator strength (0.342 and 0.695 respectively [21]), W is the Racah coefficient, F, F', J and J' are the total angular momentum and angular momentum respectively and I is the nuclear spin. Thus, in order to calculate the effective index, besides the temperature and γ, we are in need to find the momentum in the direction of propagation, and in the transverse direction. The first will specify the amount of Doppler broadening, and the later will specify the amount of transit time broadening. In waveguide terminology these momenta are the effective wave-number, β and the inverse evanescent decay length η, respectively. Higher the mode confinement results in larger β and smaller η leading to an increase in Doppler and transit time broadening, with reduced contrast. While this formalism holds for low temperatures below 450 ⌡K, corrections needs to be made for higher temperatures due to high density effects [19,20], where the local field relation is used, and the refractive index is given by the relation $n = ([1 + 3\chi]/[3- \chi])^{1/2}$. Another correction is by taking into account the self broadening effect, manifested as a broadening of the natural linewidth [19,22]. Additional correction is achieved by taking into account the perturbation of the evanescent tail due to its interaction with the vapor. The later has been found in [20] to have an effect in changing the evanescent exponential decaying wave to an oscillatory wave which in turn has an effect of frequency shifting the measured line-shapes. In our treatment, however, the range of temperature used is smaller than 450 ⌡K, and thus we take into account self broadening and local field effects but neglecting the perturbation of the evanescent tail of the optical mode. However, for the case of higher densities one needs to take into account the mutual influence between the vapor and the mode profile.

The procedure to obtain the effective index of the mode is perturbative in its nature. First, we use the finite element method simulate (FEM, Comsol Multi Physics) to calculate the fundamental TE-like mode of the structure described in Fig. 1(b). We note that although the waveguide supports both TE and TM mode, we only consider the TE mode as it has a higher fraction of its mode in the cladding region. Moreover, as TE to TM mode conversion is negligible in our structures, by launching a TE mode it is possible to consider these waveguides as practically single mode. TM mode can be also eliminated by a slight modification in waveguide dimensions.

From the mode profile we find the fraction of mode (the electric field component) which resides in the Rb cladding, which in our case is 16%. Next, we numerically evaluate the expression in Eq. (1), using ^{87}Rb and ^{85}Rb oscillator strengths and resonance frequency (D1 lines) data found for instance in [21,23], the previously simulated wave vectors in the propagation direction, β the inverse evanescent decay length η, and the density of atoms, corresponding to the temperature of 140°C. Next, we use the local field relation in order to obtain the effective complex cladding index of refraction, and use it as to represent the cladding of the waveguide. The complex effective index of refraction of the guided mode is obtained by the relation: $n_{eff,\ combined} = n_{eff} + \Gamma\Delta n_{cladding}$. Finally we use this effective index in order to propagate the mode in the waveguide, over a length determined by the interaction region, using the Beer-Lambert relation. In general, the natural width γ has been taken to be

#176246 - $15.00 USD Received 14 Sep 2012; revised 15 Nov 2012; accepted 16 Nov 2012; published 4 Dec 2012
(C) 2012 OSA

5.9 MHz. However, in the case of optically dense vapor one has to account for self broadening and surface interactions that result in additional broadening on the natural width. In our case, including the self broadening, according to [19,22], accounts to a total width of 9.4 MHz.

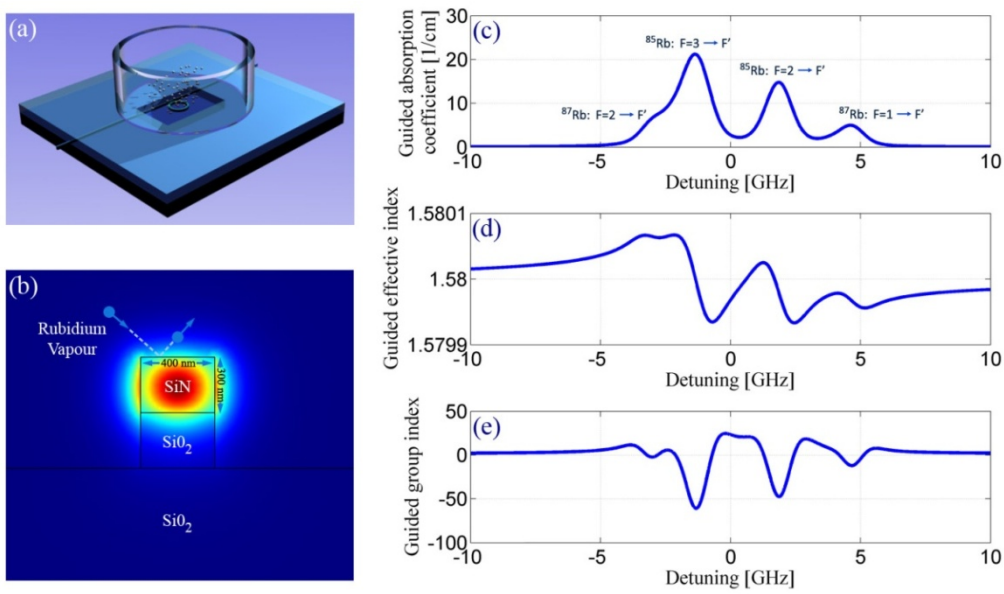

Fig. 1. **(a)** Schematic diagram of an atomic vapor cell bonded to a chip consisting of SiN MRR **(b)** Calculated TE-like electric field distribution (in absolute values) for the D1 wavelength of Rb (795 nm) superimposed on the geometry of the proposed MRR's wave guide. Rb atoms are illustrated as balisitcaly striking the surface, entering the evanescent portion of the optical mode. Plotted is the norm of the electric field. **(c)** Absorption coefficient of the fundamental waveguide mode as a function of frequency detuning **(d)** Effective index of the atomic cladding fundamental waveguide mode **(e)** Group index of the atomic cladding fundamental waveguide mode, calculated using the effective index from (d)

In Fig. 1(c) we plot the calculated absorption coefficient of the atomic cladding fundamental waveguide mode using the dimensions of 400 nm width and 300 nm height, and the above mentioned Rb temperature. The simulated effective index of the guided mode, being 1.58 gives rise to an increase in the momentum carried by the optical mode, and as a result an increased Doppler broadening. Additionally, due to the finite time of interaction in the evanescent region, being of approximately 100 nm in length, transit time broadening is evident. As a consequence, this line broadening causes an overlap of the hyperfine levels, relative to the case of a standard Rb transmission spectrum. In Fig. 1(d) we plot the real part of the effective index of the fundamental waveguide mode, where one can see the anomalous dispersion around the absorption peaks, and the normal dispersion in between these absorption peaks. The former corresponds to negative group index, and the later corresponds to positive group index. Next, we derive the group index, using the relation $n_g = n_{eff} + \omega dn_{eff}/d\omega$. This group index is shown in Fig. 1(e). One can see a maximal group index in the range of ~-60, around the resonance dips of ^{85}Rb.

Finally, we note that the aging rates and mechanisms in such recently demonstrated devices [10] are yet to be characterized. These could include the creation of a layer of Rb atoms on the SiN waveguides, which in turn will induce loss. Yet to be determined is the rate of such processes, as well as its reversible mechanism, i.e. using local heaters to detach such a layer. Nevertheless, in [10] we have reported devices who have not witnessed any degradation in their transmission in the course of several weeks.

#176246 - $15.00 USD Received 14 Sep 2012; revised 15 Nov 2012; accepted 16 Nov 2012; published 4 Dec 2012
(C) 2012 OSA

3. MRR dispersion

Before discussing the properties of the integrated system, we briefly review the dispersive properties of each of the ingredients, namely the MRR and the atomic vapor. The transfer function (being the ratio of the output field to the input field as function of frequency) of an MRR is given by [24]:

$$h(\omega) = \frac{t - ae^{i\phi_{rt}}}{1 - tae^{i\phi_{rt}}} \tag{3}$$

Whereas the intensity transfer function is given by:

$$T(\omega) = |h(\omega)|^2 = \frac{a^2 + t^2 - 2at\cos\phi_{rt}}{1 + a^2t^2 - 2at\cos\phi_{rt}} \tag{4}$$

Where t is the through coupling coefficient, ϕ_{rt} is the round trip phase, and a is the loss parameter related to the round trip loss via the relation $a = \exp(-\alpha L/2)$ (α is the power absorption coefficient per unit length, and L is the circumference of the MRR). The time delay, in a linear time invariant (LTI) system is given by the derivative of the phase of h(ω) with respect to ω. This total phase is given by [25]:

$$\Phi_{Total} = angle(h) = \pi + \phi_{rt} + \mathrm{a}\tan\left(\frac{t\sin\phi_{rt}}{a - t\cos\phi_{rt}}\right) + \mathrm{a}\tan\left(\frac{ta\sin\phi_{rt}}{1 - ta\cos\phi_{rt}}\right) \tag{5}$$

Assuming $\phi_{rt} = \omega n_{eff} L/c$ and t, a < 1, the time delay will be given by:

$$\tau(\omega_0) = \frac{L}{c}\left[n_{eff} + \left(\frac{n_{eff}t}{a-t} + \frac{n_{eff}ta}{1-ta}\right)\right] = \frac{L}{c}n_g \equiv \frac{L}{v_g} \tag{6}$$

Where n_{eff} and n_g are the effective index and the group index of waveguide, respectively. Equation (4), plotted as a function of the coupling coefficient in Fig. 2(a), expresses the dual dispersion-wise nature of the MRR. In the over-coupled regime ($t < a$), the time delay is positive and slow light is achieved, while in the under-coupled regime ($t > a$), the time delay is negative, and fast light is achieved. Effectively, one can interpret the term within the square brackets of Eq. (4) as the group index of the MRR, and the term within the round brackets as $\omega_0 dn(\omega_0)/d\omega$, in compliance with the definition of the group index, and its relation with the time delay: $\tau c/n_g = \tau v_g = L$. We now define the term transmittance-group delay product (TGDP) that is given by the group index (the square brackets in Eq. (4)) multiplied by the transmission intensity (Eq. (2)) at resonance:

$$(n_g \cdot T)\big|_{\omega=\omega_0} = \frac{a(a-t)}{(1-at)^2} + \frac{ta(a-t)^2}{(1-at)^3} \tag{7}$$

Figure 2(b) shows the TGDP as a function of the coupling coefficient. It can be shown that the region of high group index illustrated in Fig. 2(a) is accompanied with vanishing transmission. A negative optimal value of the TGDP of nearly −20 is obtained for the case of under-coupling, with t~0.995. Positive TGDP values are obtained in the over-coupled regime, where an optimal positive TGDP of about 20 is obtained for t~0.96.

#176246 - $15.00 USD Received 14 Sep 2012; revised 15 Nov 2012; accepted 16 Nov 2012; published 4 Dec 2012
(C) 2012 OSA

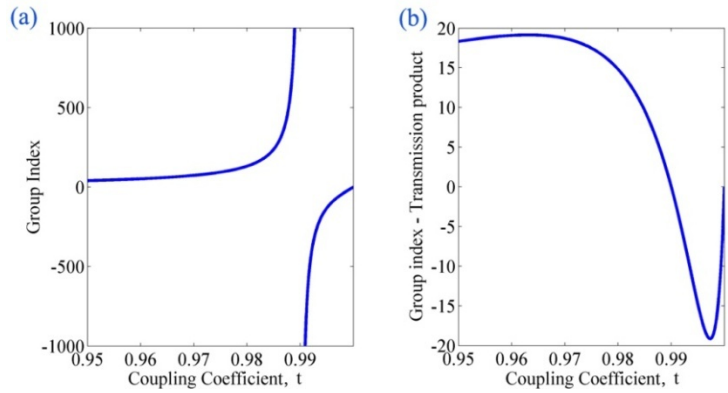

Fig. 2. (a) MRR time delay as a function of the coupling coefficient. The MRR time delay inverts its sign at critical coupling. (b): transmission-group delay product as a function of the coupling coefficient, illustrating that high values of time delay are accompanied with vanishing transmission. Optimal positive (negative) values of transmission- group delay product are obtained for over (under) coupled system. A loss parameter of a = 0.99 was assumed.

4. Combined system of atomic vapor and MRR

We now turn to the analysis of the combined MRR-atomic system. We model the device by considering the transfer function of an MRR (Eqs. (2) and (3)), using the effective index of refraction of the atomic cladding wave guide presented in section 3. Using this effective index of refraction we get the following round trip complex transfer function:

$$ae^{i\phi_{rt}} = (a_r e^{-\omega/ck_{eff}L})e^{i\omega/cn_{eff}L} \tag{8}$$

where a_r is the loss parameter of the MRR due to the structure (e.g. because of radiation loss) and $n(\omega) = n_{eff} + ik_{eff}$ is the complex effective index of refraction of the atomic cladding wave guide. We assume that the MRR's resonance coincides with the atomic resonances. In practice this condition is not easily achieved - adjusting the wavelength of the MRR within a spectral window of ~10 GHz requires high accuracy in fabrication. However, this obstacle can be mitigated, for example, by selecting appropriate MRR's following by applying thermal tunability. Additionally, we assume that the optical power within the structure doesn't exceed the saturation power, estimated to be in the nW regime. The chosen MRR's parameters, (intrinsic loss, and coupling coefficient), correspond a MRR with an extinction ratio of ~22 dB and Q factor of 12,000, both can be achieved in a realistic system.

In Fig. 3(a) we plot the transmission spectrum of a $2\pi\cdot 5.6$ μm long atomic cladding waveguide, corresponding to the round trip transmission of an uncoupled MRR having a radius of 5.6μm. The broadened Rb dips are evident. In Fig. 3(b) we plot the transmission of the combined system of the MRR and Rb vapor, as well as the standalone MRR. It can be seen that the atomic finger print is induced on the MRR's transmission. This manifests in enhanced transmission, ~40-50%. Moreover, relative to the contrast of the absorption dips in Fig. 3(a), the MRR exhibits enhanced contrast (an order of magnitude), which can be viewed as an effect of the photon lifetime in the cavity. In Fig. 3(c) we plot the MRR's overall phase delay, as a function of the frequency detuning, for the cases of an atomic cladding MRR (blue) and a standalone MRR (green). Finally, in Fig. 3(d) we plot the group index of the combined system, being the total phase derivative in respect to the frequency. An unusual time delay spectrum is achieved. At frequencies of maximal absorbance, corresponding to frequencies with enhanced transmittance, we observe a positive time delay, in spite of the fact that by itself the atomic medium inherently exhibits negative time delay. These positive time delays have a bandwidth of approximately 1GHz. In contrast, at the frequencies between the

#176246 - $15.00 USD Received 14 Sep 2012; revised 15 Nov 2012; accepted 16 Nov 2012; published 4 Dec 2012
(C) 2012 OSA

atomic lines large negative group index is observed, although the atomic medium in these frequencies exhibits positive time delay, often exploited for slow light experiments [26].

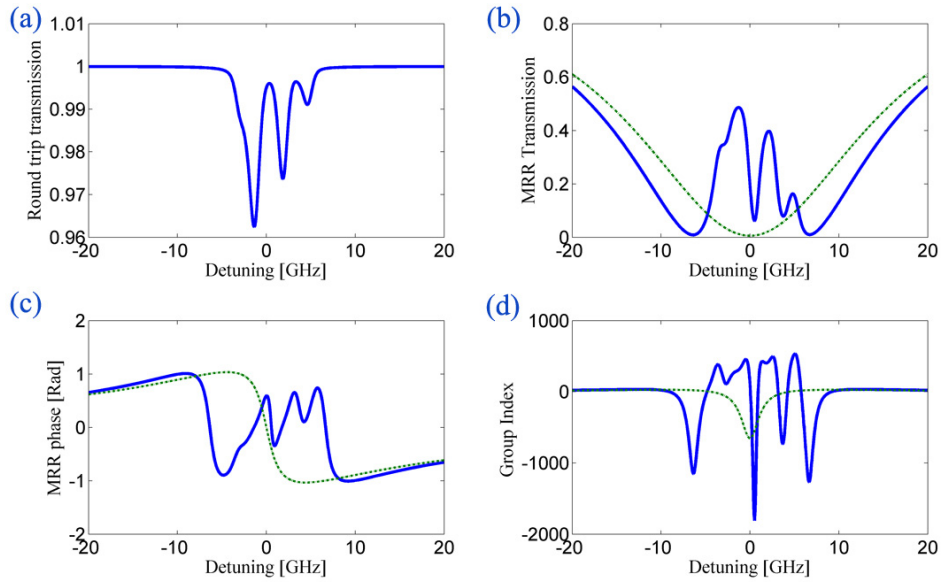

Fig. 3. **(a)** Round trip transmission (normalized linear scale) of the atomic cladding wave guide which constitutes the MRR **(b)** Combined (blue) and standalone (green) MRR transmission as a function of frequency detuning **(c)** Combined (blue) and standalone (green) MRR phase delay as a function of frequency detuning **(d)** Combined (blue) and standalone (green) MRR's group index as a function of frequency detuning

In order to understand these results we first evaluate the transmission of an atomic cladding wave guide consisting of a single resonance, coinciding with the MRR resonance. For the purpose of comparison we assume similar parameters for the MRR as before. The device's transmission in the case of coinciding resonances takes the following form:

$$T(\omega) = \left(\frac{a - t}{1 - at} \right)^2 \tag{9}$$

with the above mentioned combined new loss parameter given by $a = a_r e^{-i\,\omega/ck_{eff}L}$. In Fig. 4(a) we show the transmittance of the ACWG MRR (blue) and the standalone MRR (green). One can see that the resonator with the loss induced by the vapor perturbs the transmission significantly, and creates a peak or dip in the transmission. This hole/dip burning in the MRR's spectrum is due to our choice of a MRR with a wider line-width compared with the linewidth of the atomic media. Hence, the standalone MRR defines an envelope transmission for the combined structure in frequencies that are significantly detuned from the absorption of the vapor. The turning point between obtaining a peak or a dip in transmission occurs at the intersection between both curves. We demonstrate two different regimes of coupling, that correspond to distinctly different transmission and group index spectra. In order to isolate the fundamental phenomena, we focus on the excitation of the ^{85}Rb F = 2 overlapping transitions. In Fig. 4(b) we plot the MRR's transmission in the over coupled regime, for coupling values of 0.95, as denoted by the squares in Fig. 4(a). One can clearly see the dip created in the background MRR's transmission. In contrast, in Fig. 4(c) we are operating in the under coupling regime, i.e. r = 0.991 (shown as circles in Fig. 4(a)) and as a consequence a peak in transmission is created. In both cases, the peaks and dips are accompanied with positive or

#176246 - $15.00 USD Received 14 Sep 2012; revised 15 Nov 2012; accepted 16 Nov 2012; published 4 Dec 2012
(C) 2012 OSA

negative group index's, illustrated in figure d and e. This phenomenon will be explained shortly in the next paragraph.

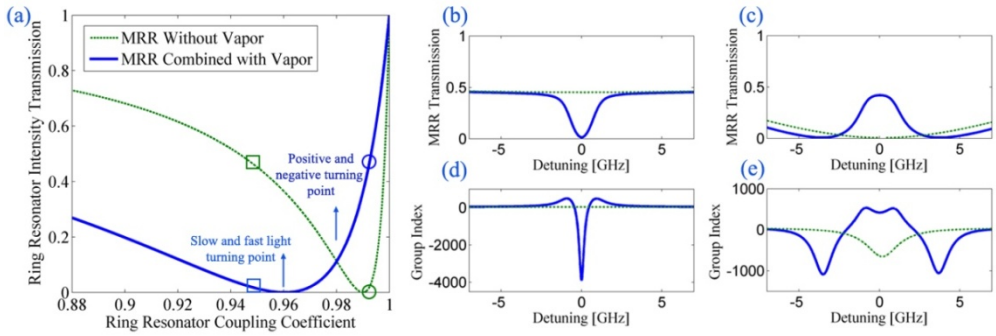

Fig. 4. **(a)** Combined (blue) and standalone (green) MRR transmission as a function of coupling coefficient. Illustrated are the different turning points: the negative (dip) and positive (peak) turning point and the turning point between slow and fast light. **(b)** MRR transmission in the over-coupled regime **(c)** MRR transmission in the under-coupled regime **(d)** MRR group index in the over-coupled regime **(e)** MRR group index in the under-coupled regime. In all figures, the dashed green figures correspond to the standalone MRR, and the blue figures to the combined system.

Next, we obtain an analytic expression for the time delay of the combined system. The phase delay of the combined system can be written in the same form as in Eq. (3), with the exception that the phase shift and loss parameter are dispersive, i.e vary as a function of frequency $\Phi = f\,(\phi(\omega), a(\omega), t)$. The round trip phase at the vicinity of an atomic resonance can be written as follows:

$$\phi_{rt} = \frac{\omega L}{c} n_{eff}(\omega) \approx \frac{\omega L}{c}\left(n_{eff}(\omega_0) + \frac{dn_{eff}}{d\omega}\Delta\omega\right) \tag{10}$$

with the time delay being the derivative of the of the phase delay:

$$\tau(\omega) = \frac{d\Phi_{total}(a,\phi_{rt})}{d\omega} = \frac{d\Phi_{total}}{d\phi_{rt}}\frac{d\phi_{rt}}{d\omega} + \frac{d\Phi_{total}}{da}\frac{da}{d\omega} \approx \frac{d\Phi_{total}}{d\phi_{rt}}\frac{L}{c}\left(n_{eff}(\omega_0) + \frac{dn_{eff}}{d\omega}\Delta\omega + \omega\frac{dn_{eff}}{d\omega}\right) + \frac{d\Phi_{total}}{da}\frac{da}{d\omega} \tag{11}$$

At resonance ($\Delta\omega = 0$) the terms multiplied by the frequency difference and the derivative of $a(\omega)$ with respect to the frequency vanish, and we obtain a simplified relation for the time delay of the combined system:

$$\tau(\omega_0) = \tau_{ring}(a(\omega_0)) \cdot \left(n_{eff}(\omega_0) + \omega_0 \frac{dn_{eff}(\omega_0)}{d\omega}\right) = \tau_{ring} \cdot n_{group,eff} \tag{12}$$

As can be seen, the time delay of the combined system is very different from the time delay of the standalone MRR. First, τ_{ring} differs from the time delay of the standalone MRR. This is because of the higher loss due to the absorption of light by the atoms. In addition, the delay is multiplied by the group index of the mode (being a hybrid mode of the wave guide and the atoms). This result, also implies a counterintuitive phenomena in which an MRR resonance being of width larger than the atomic absorption lines, still has a pronounced effect on the overall group index. This however can be explained by the fact that the MRR's group index is dependent on the relation between the coupling conditions and the MRR's intrinsic loss, rather than being scaled with the resonance linewidth. It can also be understood by recalling that the

#176246 - $15.00 USD Received 14 Sep 2012; revised 15 Nov 2012; accepted 16 Nov 2012; published 4 Dec 2012
(C) 2012 OSA

MRR's transmission and phase delay are not connected through Kramers Kronig relations [27].

Using Eq. (12), we can now turn to explain our findings in Figs. 3 and 4. Around a resonance line of Rb, the group index of the waveguide mode is negative. However, the time delay of the ring depends on the coupling strength, i.e. on whether the MRR is over coupled or under coupled. As a consequence, the time delay of the combined MRR can be either negative or positive, resulting in a negative time delay (fast light) at the under-coupled region and a positive time delay (slow light) at the over-coupled region. The turning point between these two cases is marked in Fig. 4(a). Thus, from the point of view of the embedded material, the combined structure has the feature of altering it's time delay sign, depending on whether the system is over coupled or under coupled. From the point of view of the MRR, the embedded material has the feature of reversing the order of the negative and positive time delay, depending on the coupling coefficient, i.e. fast light will be achieved in the over-coupled regime, and slow light will be achieved in the under-coupled regime. These two distinct modes of operation are shown in Figs. 4(d), 4(e) showing the over coupled fast light regime and the under coupled slow light regime. In the former case one achieves a negative group index of a few thousands, accompanied with a −20dB transmission, and in the later one achieves positive group index of a few hundreds, accompanied with −3dB transmission. The under coupled regime corresponds to the scenario illustrated in Fig. 3. However, in Fig. 3 we have an additional phenomena, which is attributed to the positive group delay the atoms provide, in between the absorption dips. In such a case, the group index of the ACWG is positive, and that of the MRR is negative (being under coupled) and thus negative index of about ~1800 is achieved with −12dB transmission.

We now turn to analyze the broadening mechanisms in the combined transmission spectrum. It is clear from Fig. 3(b) as well as Fig. 4(c) that the width of the peaks in the transmission spectrum are broadened compared with the case of a bare ACWG (Fig. 3(a)). Careful inspection of the ^{85}RB F = 2 transmission lines in Fig. 4(c) reveals that the full width half maximum of the peak is 2.7 GHz, whereas the Doppler and Transit time broadened width of the ^{85}RB F = 2 transmission overlapping lines is approximately 1.27 GHz. In general, the large negative group index induces a line narrowing [28–31] in the MRR resonance. However, this effect is masked by the absorption accompanied with this negative group delay, yielding a "flattop" resonance. This is demonstrated in Fig. 5, where we first illustrate the in Fig. 5(a) the round trip optical density being the product of the MRR's circumference by the power absorption coefficient. Next, in Fig. 5(b) we plot MRR's effective index. Finally, in Fig. 5(c) we show the transmission spectrum of the atomic cladding MRR (blue), taking into account the effect of both dispersion and loss. To provide further insight we also plot the expected transmission spectrum considering each effect by itself, with the red curve corresponds to the lossless case and the cyan curve corresponds to a non dispersive waveguide. It is clear that that for the case of lossless and dispersive device, significant line narrowing is observed owing to the large group index. This narrowing is in the spectral range where the dispersion is linear, as can be seen in Fig. 5(b). However, when we "turn off" the dispersion, and "turn on" the absorption we mask this effect, due to the perturbation of the extinction ratio of our MRR as explained before.

#176246 - $15.00 USD Received 14 Sep 2012; revised 15 Nov 2012; accepted 16 Nov 2012; published 4 Dec 2012
(C) 2012 OSA

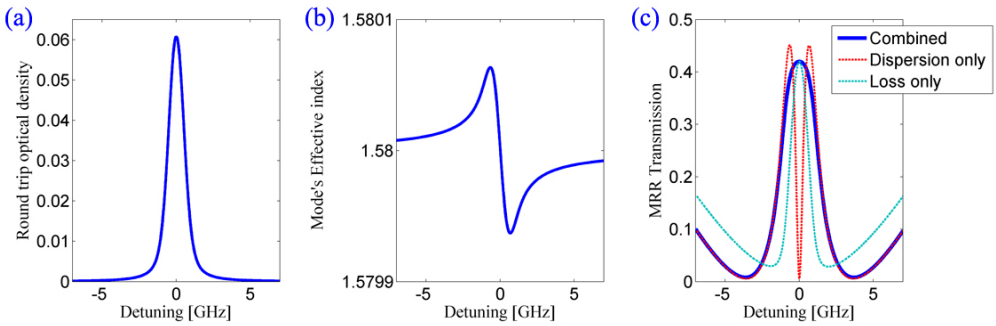

Fig. 5. **(a)** Round trip optical density **(b)** Atomic Cladding wave guide effective index **(c)** MRR transmission in the case we have an atomic cladding wave guide MRR (blue), in the case we have an fictitious atomic cladding wave dispersion only (red), the case we have a fictitious atomic cladding with absorption only (cyan).

Before concluding, it is important to discuss the role of temperature in our system. Clearly, the temperature degree of freedom plays a role in tuning the MRR as well as in controlling the density of atoms. As we have seen before, the resonance of the atomic media, has to roughly coincide with the resonance of the MRR. Due to fabrications imperfections, the actual MRR's resonance wavelength may deviate from the designed value. A tuning mechanism, such as using the thermo-optic effect would ideally overcome this problem; however tuning over a full spectral range in small diameter MRR's is not feasible as it requires heating in the range of hundreds of degrees. While today's commercial fabrication capabilities allows to control the resonance wavelength to within a nanometer and even less, this still requires a substantial thermal heating for aligning the wavelength of the MRR with that of the atomic transition. Further device tunability can be achieved e.g. by using approaches such as UV trimming [32], and applying pre-selection step to choose devices with their resonance wavelength as close as possible to the target wavelength. After doing so, further fine tuning of the resonance wavelength can be achieved by thermal tuning. The temperature stability that is required to maintain resonance frequency stability of ~1 GHz in the MRR is ~0.1⎫C. As to the vapor density, also controlled by the temperature, a deviation of 5 degrees corresponds to density changes of 25 percent, accounting for a small change in the transmission and group index. (~5 percentage to the transmission, and ~10% to the group index). Thus temperature stabilities in the range of 0.1⎫C is expected to be sufficient for stabilizing both the MRR resonance frequency and the atom density.

Finally, we discuss the various parameters and their role for optimization of the devices performance. In order to maximize the transmission contrast, one should optimize four major parameters, namely the coupling coefficient, the atomic density, the MRR's loss and the MRR's circumference. The optimization process will bring these four parameters to a point where a maximal difference between the two curves presented in Fig. 4(a) will be reached. The same parameters are also relevant for the optimization of the group index, however naturally their role in the optimization is different. In order to maximize the group index we should maximize the product of the group index of the MRR and the group index of the atoms (Eq. (12)). Unfortunately, increasing the group index of the atoms by simply increasing their density (to first order the atomic group index scales linearly with the atomic density) will not necessarily increase the overall ACWG MRR group index, because the relation between the coupling coefficient and the total loss of the ACWG MRR is now modified. Therefore, a global optimization approach is needed in order to maximize both the transmission and the group index of the combined system.

#176246 - $15.00 USD Received 14 Sep 2012; revised 15 Nov 2012; accepted 16 Nov 2012; published 4 Dec 2012
(C) 2012 OSA

5. Summary

We proposed and analyzed the transmission and time delay properties in a hybrid system consisting of structural resonance and material resonance. Specifically we examined the system of fine structure transitions of the D1 line of Rb embedded above a silicon nitride MRR. We have used an effective susceptibility in order to calculate the MRR's atomic cladding wave guide effective (complex) mode, taking into account different unique broadening mechanisms akin to our system. We analyzed the transmission of such a hybrid system, and found that it should be possible to significantly enhance the contrast of the Rb peaks. In addition we found that such a combined system may exhibits negative and positive enhanced time delays, as well as spectral holes and dips in the transmission. Specifically, in the under-coupled regime, one can achieve positive time delay accompanied with enhanced transmission peak, as well as negative time delay with somewhat enhanced transmission. The proposed platform is promising for generating slow and fast light on chip, with the advantage of relatively simple probing of the atomic system, reduced footprint, high tunability (e.g. by changing the density of atoms via temperature or by the use of optical pumping), and relatively high delay-transmission product. In addition to the dispersive properties, the combination of Atomic Vapor and a MRR can support non-linear interactions at low intensities [10–12], due to the enhancement of the energy density in the MRR. Finally, due to the high energy density of the guided mode interacting with the vapor, the power threshold for nonlinear interactions is reduced significantly, paving the way for important on chip applications such as few photon switching.

#176246 - $15.00 USD Received 14 Sep 2012; revised 15 Nov 2012; accepted 16 Nov 2012; published 4 Dec 2012
(C) 2012 OSA